ACS Photonics

ACS Editors' Choice

Article

pubs.acs.org/journal/apchd5

Terms of Use

Beaming Visible Light with a Plasmonic Aperture Antenna

Jue-Min Yi,[†,⊥] Aurélien Cuche,[‡] Eloïse Devaux,[†] Cyriaque Genet,[†] and Thomas W. Ebbesen*[,†]

[†]ISIS, University of Strasbourg and CNRS (UMR 7006), 8 Allée Gaspard Monge, 67083 Strasbourg, France

[‡]CEMES, University of Toulouse and CNRS (UPR 8011), 29 Rue Jeanne Marvig, 31055 Toulouse, France

ABSTRACT: We investigate experimentally the parameter space defining, in the visible range, the far-field diffraction properties of a single circular subwavelength aperture surrounded by periodic circular grooves milled on a metallic film. Diffraction patterns emerging from such an antenna are recorded under parallel- and perpendicular-polarized illumination at a given illumination wavelength. By monitoring the directivity and the gain of the antenna with respect to a single aperture, we point out the role played by the near-field surface plasmon excitations. The results can be analyzed through a Huygens–Fresnel model, accounting for the coherent interaction between the field radiated by the hole and the plasmonic field, propagating along the antenna surface and diffracted away in free space.

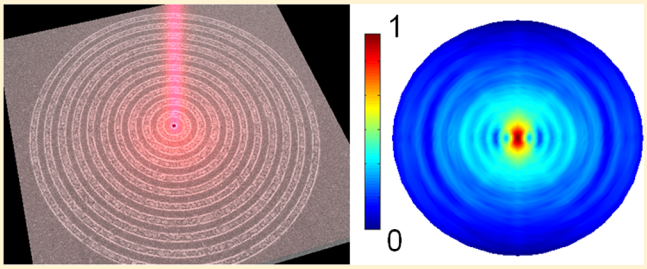

KEYWORDS: *subwavelength aperture, surface plasmons, nanoantenna, antenna gain, antenna directivity*

Tiny apertures perforated through metallic screens have recently revealed unique optical properties, involving surface plasmon (SP) resonances and associated local field enhancement effects.[1] Because of a Fourier relation ($\Delta k \approx 1/\Delta x$), the angular distribution Δk of the signal diffracted in the far field through a single subwavelength aperture ($\Delta x \ll \lambda$) is very broad, meaning that relevant near-field features of the aperture are lost after propagation.[2] Nanostructuration around the aperture is therefore necessary when aiming at controlling light properties in free space. Of particular interest is the bull's eye (BE) system, consisting of concentric grooves engraved on the surface a metallic film around a subwavelength aperture perforated through the film. It was shown experimentally that the electromagnetic (EM) field emerging from a BE can be directed and beamed in free space within a limited solid angle, revealing its unique properties, including extraordinary optical transmissions in narrow spectral windows centered on tunable SPP resonances.[3−7] Many experimental and theoretical studies have since looked at some of the BE features in different regions of the EM spectrum from near-infrared to microwaves.[8−13] It also has been discussed how these concepts can be transposed to thermal,[14] matter,[15] or sound wave[16] areas, exploiting the generality of the surface wave concept. For the sake of simplicity however, most works have studied unidimensional structures and/or far from the visible range. Despite the limited exploration of the BE parameter space, such systems have nevertheless been successfully applied to semiconductor laser diodes[17] and cascade lasers,[11,18] taking advantage of the beaming in order to collimate the output light efficiently.

One overlooked but key aspect of the complex BE transmission mechanism is the role of the EM polarization. That polarization dynamics is central to BE properties can be seen from recent work in the context of chiral and singular optical issues.[19,20] The aim of this article is to provide, in the visible range, the first extensive experimental study of the polarization dependence of the diffractive properties of a cylindrical BE. Our strategy is to exploit the analogy between a BE and a nanoantenna in order to investigate the role of the incident EM polarization and the SP excitations involved in the emission properties of a BE.

An antenna is defined by its ability to convert efficiently free-propagating optical modes to localized energy and vice versa. The large majority of plasmonic antennas are based on localized resonances excited on small metallic structures.[21−24] Nevertheless, by coupling efficiently to radiative mode in the far field, delocalized and propagating SP modes (at work within the cavity defined by the BE area) lead to strong beaming effects, which can be understood as an antenna behavior using a reciprocity argument. Such a behavior has actually been discussed recently at the level of single emitter ensembles coupled to BE, allowing for enhancement and spatial control of their emission.[25,26]

As we will show, the concepts brought in from antenna theory turn out to be particularly relevant for analyzing the experimental angular distributions of the light diffracted in three dimensions through the BE. To do so, we use a highly stable and high-resolution homemade goniometer with a BE carefully aligned along the optical axis of the setup and precisely positioned in its (x,y) plane. The diffracted light is collected in the far field by a multimode fiber coupled to a spectrometer, scanning an angular sector $\theta = -60°$ to $+30°$ in the (x,z) plane. We illuminate the BE with a linear parallel polarization along the x-axis with the azimuthal angle $\varphi = 0°$ (lying in the detector plane) or a perpendicular polarization along the y-axis with

Received: November 29, 2013
Published: March 5, 2014

 © 2014 American Chemical Society

polar angle φ = 90° (lying in a plane perpendicular to the detector one), with no depolarization induced by the setup.[2]

The BE consists of a cylindrical subwavelength hole of diameter d surrounded by circular concentric grooves (period P, width w, depth h, and distance between central hole and first groove a). Using a focused ion beam, the hole and the grooves are respectively milled through and on a Ag metal film of thickness 300 nm (h) deposited on a glass substrate (thickness 1 mm) (Figure 1a and c). A Gaussian beam emitted from a

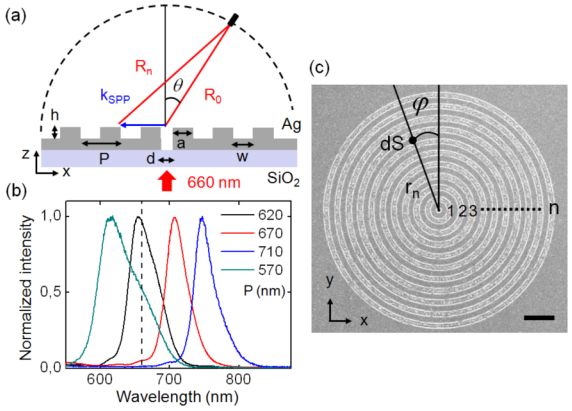

Figure 1. (a) Scheme of the antenna geometry with the relevant parameters. (b) Antenna spectra recorded under collimated white light illumination for four different groove periodicities. The laserline λ_L at 660 nm is indicated by the black dashed line. (c) SEM image of a BE. The dark central hole has a diameter d = 300 nm. Scale bar represents 1 μm.

single mode laser diode at a wavelength λ_L = 660 nm is linearly polarized and weakly focused at normal incidence on the sample by a microscope objective (10×, NA = 0.3). At this wavelength, the propagation length of SP, $l_{SP} = 1/2\mathrm{Im}[k_{SP}]$, is expected to be 25 μm on a perfectly flat Ag film, due to ohmic losses in the metal given by the imaginary part of the SP wave vector. It is worth noting at this stage that the illumination numerical aperture (NA) and the refractive index of the substrate do not have any impact on the recorded diffraction patterns. Indeed, the transmission process through a subwavelength hole milled in a thick opaque film (taking a perfect electric conductor (PEC) approximation with the hole radius enlarged by one skin depth) is controlled, under quasi-normal incident illumination, by the fundamental waveguide mode TE_{11} of the hole, which optically decouples both surfaces of the thick metallic film[2] (or HE_{11} if a Drude model that includes intrinsic losses is used to describe the opaque film[27]). We recall from ref 2 that the diffraction patterns are angularly sensitive to the groove depth and the hole diameter, which are thus constant parameters with h = 80 nm and d = 300 nm. We also keep the groove width constant at w = 200 nm. These values correspond to an optimized geometry when the antenna is used as a collector under white light illumination[4,5].

As seen in Figure 1b, the BE antenna is resonant with λ_L when the low-energy mode, which displays a symmetric profile for the electric field, is excited for P = 620 nm.[28] In agreement with previous work, a strong beaming is observed at resonance. This phenomenon stems from a cumulative interference effect between the broad beam diffracted from the central hole and the SP waves, launched by the hole and diffracted away in the far field by each groove.[8,29] Figure 2a and b clearly reveal, both for parallel and perpendicular polarizations, the progressive

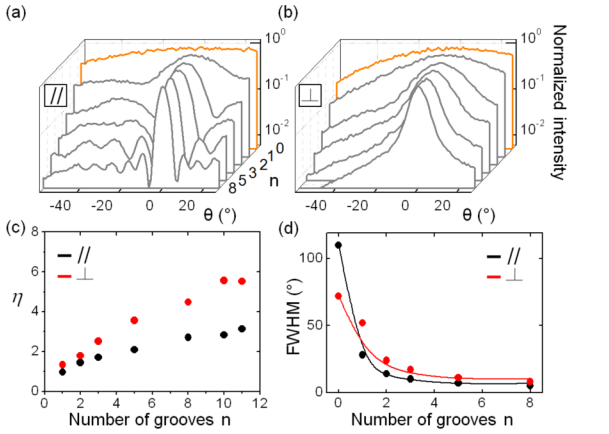

Figure 2. Normalized diffraction patterns in logarithmic scale depending on the groove number n, under parallel (a) and perpendicular polarizations (b). Antenna integrated enhancement factor η (c) and main lobe fwhm (d) as a function of groove number n for parallel (black dots) and perpendicular polarization (red dots). In (d) experimental data are compared to theoretical predictions (solid lines).

transition between the single hole (SH) regime and the BE antenna as n is increased gradually, giving the BE antenna the capacity to concentrate light in small solid angles.

A quantitative approach to this phenomenon consists, in an antenna theory framework, in defining the integrated enhancement factor η,

$$\eta = \frac{\int I(\theta)\,\mathrm{d}\theta}{\int I_{SH}(\theta)\,\mathrm{d}\theta} \quad (1)$$

by integrating the BE angle-dependent transmitted intensity $I(\theta)$ over the angular sector $[-60°;60°]$, normalized by the same quantity defined on a corresponding SH. Clearly, η evolves almost linearly with n, illustrating the aforementioned cumulative effect. Interestingly, η cannot be associated only with the contribution of SP modes decoupled to the far field. Evanescent waves launched at the hole position and scattered away in the far field by the grooves (within a large set of in-plane k wave vectors) also contribute to the high values reached by η. For a resonant BE, the different EM contributions are in phase along the optical axis (θ = 0), leading to the observed intense beaming. This buildup is accompanied by a dramatic reduction of the full width at half-maximum (fwhm) of the angular pattern, as seen in Figure 2c and d. This corresponds to a narrowing of the angular emission, highlighting the BE antenna efficiency to convert the EM energy localized at the hole to free-propagating modes.

The number n of grooves therefore rules the total efficiency of the far-field SP conversion and thus the optical performance of the antenna itself. It is worth noting that a maximum value of η and a minimum one for the divergence are reached for n = 10 before saturation. Although the theoretical SP propagation length at λ_L on a Ag film is expected to be close to 25 μm, the saturation observed at n = 10 corresponds to a distance of only 6.2 μm. This value gives a good estimation of the effective propagation length on a highly dissipative structured surface due to scattering losses. It corresponds to an effective near-field spatial coherence length $l_c = nP$ equal to the total source size.

The cumulative interpretation of the beaming complies well with a Huygens–Fresnel (HF) point of view, where any

dx.doi.org/10.1021/ph400146n | ACS Photonics 2014, 1, 365–370

component of the electric field $E(P_\theta)$ results from the interference of the direct transmission and the scattering from the grooves at any detection point P_θ in the far field at a distance R_0 from the SH and R_n from the nth groove; see Figure 1b. Within such a point of view, the total intensity measured in the detection plane is modeled by

$$I(\theta) \approx \left| E_0 \frac{e^{ikR_0}}{R_0} + \sum_n \alpha(n) \oint_g u(r_n) \frac{e^{ikR_n}}{R_n} ds \right|^2 \quad (2)$$

where the first term involves the direct transmission through the hole and the second term, summed over the n grooves, corresponds to the SP field generated at the hole and scattered in the far field on each groove. The SP scattering process is given by a simple scattering coefficient,

$$\alpha(n) = \gamma \cos(\theta)\, e^{-r_n/l_c} \quad (3)$$

where l_c is the effective coherence length extracted from experimental data. Accounting for additional scattering losses, this effective length must be smaller than the theoretical SP propagation length $l_{SP} = 1/2\mathrm{Im}[k_{SP}]$, which corresponds only to attenuation by ohmic losses in the metal through the imaginary part of the SP wave vector. The (real) parameter γ gives the scattering strength of the process connected to the SP field amplitude $u(r_n)$ evaluated at the nth groove by a cylindrical propagator corresponding to the propagation of the SP field amplitude from the central hole to the groove with radius r_n:

$$u(r_n) = E_{SP} \cos(\varphi - \varphi_0) \frac{e^{i\mathrm{Re}[k_{SP}]r_n}}{\sqrt{r_n}} \quad (4)$$

Here, $E_{SP} = \tilde{\gamma} E_0$ is the SP amplitude launched at the hole, considering (using a reciprocity argument) an SP excitation efficiency $\tilde{\gamma}$ at the hole and assuming, through a reciprocity argument that $\tilde{\gamma} \approx \gamma$, in other words that launching and out-coupling of SP modes have the same efficiency. The angles φ and φ_0 give the propagation directions of the surface plasmon and the incident electric field, respectively.

This model leads to an interference phase difference expressed as

$$\Delta\Psi = k(R_n - R_0) + \mathrm{Re}[k_{SP}]r_n + \Phi \quad (5)$$

the first term stemming from the difference in free space propagation optical path shown in Figure 1a, the second one accounting for the phase acquired by the SP wave propagating along the Ag surface from the hole to the nth groove, and the third one an additional phase.

The ability of this model to recover the narrowing of the angular emission is clearly seen in Figure 2d from the good agreement between the fwhm experimental points and the HF modeling, giving ($\gamma^2 = 0.3$, $\Phi = \pi$, $l_c = 8 \times P \approx 5$ μm) as best fitting parameters used in all following comparisons. The model also describes properly the polarization-dependent diffraction pattern outside resonance with a different value of P. In Figure 3a and b, the normalized experimental and theoretical diffraction patterns recorded for a BE antenna with $P = 710$ nm are plotted for both polarizations. The data reveal that the antenna does not confine the light anymore in a single narrow lobe along the optical axis but exhibits a more complex pattern with multilobes. This multilobe signature and the ratio between diffraction patterns for parallel and perpendicular polarizations show how critical the choice of periodicity is with

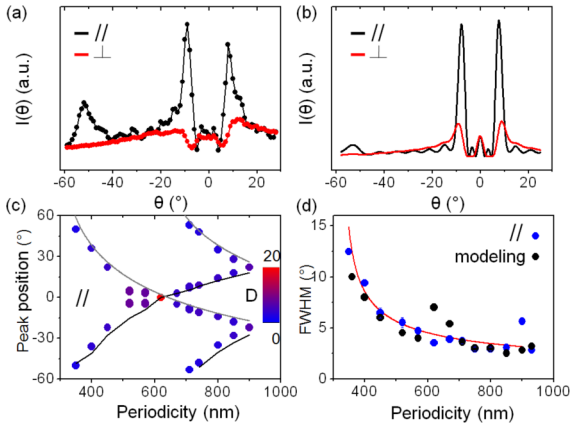

Figure 3. Experimental (a) and theoretical (b) normalized diffraction patterns at $P = 710$ nm under parallel (black curve) and perpendicular (red curve) incident polarizations. (c) Angular peak positions as a function of P. The color scale bar is related to the directivity D. Grating theory is plotted with gray solid lines for the first and second order ($m = 1$ and 2). Predictions from the Huygens–Fresnel model are plotted as a black solid line. (d) Experimental and theoretical fwhm's for different periodicities. The red solid line corresponds to the angular divergence of a primary source given by diffraction theory.

respect to the illumination λ_L in the BE angular emission properties. Again, the data are well reproduced by our model, confirming the relevance of this simple approach in order to catch the underlying physical mechanisms at play in the antenna emission process.

We also note that the results presented in Figures 2 and 3a,b clearly show that stronger effects occur when the polarization and acquisition plane are aligned, i.e., for parallel polarization. The explanation is directly related to the field distribution of SP waves launched by the central subwavelength aperture. This field distribution leads to an in-plane intensity pattern with an azimuthal profile $\propto \cos^2 \varphi$ (see eq 4) with maxima along the incident polarization.[30] It thus turns out that the effect has the highest amplitude when the direction of SP propagation is within the acquisition plane. Keeping the other geometrical parameters constant ($a = P$ and $n = 8$), the comparison can be systematically extended to other values of P.

The evolution of the peak positions extracted from the diffraction patterns measured for parallel polarization is also remarkably simple. These positions are plotted in Figure 3c for different values of P and can be compared in a straightforward manner with a grating law, $\mathrm{Re}[k_{SP}] = k_0 \sin\theta \pm mG$ (gray line), for such periodic structures (for first $m = 1$ and second $m = 2$ orders) with a grating vector $G = 2\pi/P$ and the (air) wave vector $k_0 = 2\pi/\lambda_L$. The SP dispersion relation $\mathrm{Re}[k_{SP}] = k_0 \mathrm{Re}[\varepsilon_d \varepsilon_m/(\varepsilon_d + \varepsilon_m)]^{1/2}$ is determined, as usual, from the permittivities of the dielectric (air) ε_d and the metal (Ag) ε_m film forming the interface. The experimental points, in good agreement with our model, show a small deviation that can be explained by a slightly underestimated period P involved or a too simple SP dispersion relation when considering the patterned surface.

To obtain further insight into the performances of the system, it is interesting to quantify a directivity D and a gain G of the BE, since these two parameters are the most important ones for an antenna. The directivity

dx.doi.org/10.1021/ph400146n | ACS Photonics 2014, 1, 365–370

$$D = \frac{P_{max}(\theta, \varphi)}{P_{av}(\theta, \varphi)} \propto \frac{I_{max}(\theta, \varphi)}{I_{av}(\theta, \varphi)} \quad (6)$$

defined as a dimensionless ratio of the maximum power density P_{max} to its averaged value P_{av} in the far field, quantifies the ability of the antenna to radiate the EM field in a specific region of space. The gain

$$G = \frac{P^{BE}_{max}(\theta, \varphi)}{P^{SH}_{max}(\theta, \varphi)} G^{SH} \propto \frac{I^{BE}_{max}(\theta, \varphi)}{I^{SH}_{max}(\theta, \varphi)} G^{SH} \quad (7)$$

is given as the dimensionless ratio of the maximum power density P^{BE}_{max} emitted by the BE to the maximum power density P^{SH}_{max} transmitted through a reference antenna, multiplied by the gain of that reference antenna. Since we aim at comparing the efficiency of the BE as an aperture antenna, we take the single hole as the reference antenna and take $G^{SH} = 1$ as a normalized SH gain. This is justified because a SH can be considered as a basic dipolar antenna, with quasi-isotropic emission,[2,31] and G can therefore express quantitatively the efficiency difference between the SH and the BE.

In Figure 3c, we provide the experimental one-dimensional directivity for each lobe, through the color scale bar, with $\varphi = 0$ fixed. As expected, the data show unambiguously that the highest directivity ($D = 20$) is reached in a single lobe pattern, when the antenna is resonant with λ_L. For periodicities close to this value, even if diffraction patterns show two peaks, D still has a relatively high value ($D \approx 10$). Far from resonance, D falls, illustrating the poor efficiency of the antenna in these regimes.

It is particularly interesting to compare the respective evolutions of the directivity D of the antenna and the (fwhm) divergence of its main lobe as a function of the period P. While D is clearly driven by the spectral position of the SP resonance, the angular width of the main lobe (even off-axis) decreases with P, as seen in Figure 3d. According to diffraction theory, the evolution of the angular (fwhm) divergence $\Delta\theta$ of an HF primary source is expected to fall as $\Delta\theta \propto \lambda_L/(l_c \cos\theta)$, where $\cos\theta$ is a projection term accounting for off-axis emission lobes and l_c is the effective near-field spatial coherence length of the source. The experimental data remarkably follow this evolution, as observed in the same figure (Figure 3d). Because the spatial coherence length associated with an HF source is related to the size over which the light is emitted coherently in the far field, the good agreement shows that the diffraction properties of the whole BE antenna, although being made of an assembly of individual grooves that already act as many coupled coherent secondary sources, can be describe as a primary source in the HF diffraction theory framework.

The antenna performances can be characterized from a different point of view when two-dimensional (2D) diffraction maps are acquired in Figure 4a. We experimentally reconstructed these 2D maps by gathering 1D diffraction patterns over $\varphi = [0;2\pi]$ with an increment of $\delta\varphi = 1°$. As discussed before, these data demonstrate the extraordinarily high directivity of the BE antenna at resonance with a divergence (fwhm) of only 4.32° for parallel polarization and 7.41° for perpendicular polarization. The data also confirm, by comparing the x and y directions, that the SP near-field distribution rules the profiles of the far-field emission lobes.

Just as the BE antenna reaches at resonance its highest directivity compared to a SH, as presented in Figure 3c, the gain G estimated along the optical axis ($\theta = 0$) reaches its highest value at resonance, with an evolution displayed in Figure 4b as a function of the antenna periodicity. From a huge enhancement of ca. 40 compared to the SH, the gain stays surprisingly high off-resonance, with an oscillating value around 8. Globally, the amount of light converted in the far field is definitively higher for a BE antenna than a SH, independently of the resonant condition. This effect is attributed again to a constant contribution of both scattered SP modes and evanescent waves (independent of the period). Indeed, the energy fed in surface modes and the light directly transmitted to the far field by the aperture being the same between SH and BE, the continuous increase in gain can therefore only be due to SP and evanescent near-field contributions which cannot be radiatively back-converted in the absence of grating in the SH case. This explains why the gain G can be higher than the directivity D for this category of near-field antennas, unlike classical antennas.[32]

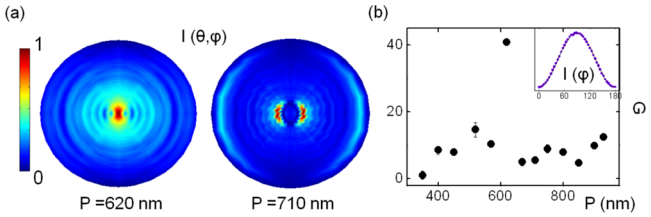

Figure 4. (a) Normalized 2D diffraction patterns for two different periodicities P = 620 nm and P = 710 nm. (b) Antenna gain G as a function of P for $\theta = 0$. Inset: Intensity at the peak angle of the bull's eye as a function of the azimuthal angle φ with a period fixed at P = 710 nm.

At this stage, we stress that the analyzed results have been obtained choosing the distance between central hole and first groove a equal to the period P. Obviously, this parameter a can act as an additional degree of freedom for controlling the antenna properties, since it fixes the phase relation between the direct transmitted light and the scattered SP field. As understood from the HF model, the antenna diffraction properties are directly related to this phase, which by tuning leads to constructive and destructive interferences in the far field due to different coherent interactions between the different EM contributions. This is indeed observed in Figure 5a, where the diffraction patterns of resonant BE antennas are displayed for different values of a under parallel and perpendicular incident polarizations, keeping all geometrical parameters constant. As expected, experimental data show unambiguously that the cavity size a strongly affects the angular patterns. For $P < a < 1.5P$, the one-lobe signature is progressively replaced by a two-lobe pattern due to the onset of a destructive interference along the optical axis. When a gets closer to $1.5P$, the axial beaming of light is observed again. The peak position evolution is perfectly symmetric with respect to this value, and the antenna shows quasi-periodic diffraction patterns with a periodicity given by a half-integer multiple of the resonant periodicity P.

Although ohmic and scattering losses should degrade the antenna efficiency when increasing the size of the structure (typically above l_c), Figure 5 puzzlingly reveals that the antenna directivity D keeps increasing when the central cavity is enlarged. This is accompanied by a drastic reduction of the angular divergence of the emission lobe. We emphasize that it is possible to reach a spectacular regime where the fwhm of the main lobe goes down to only 1°, confirming the crucial role

dx.doi.org/10.1021/ph400146n | ACS Photonics 2014, 1, 365−370

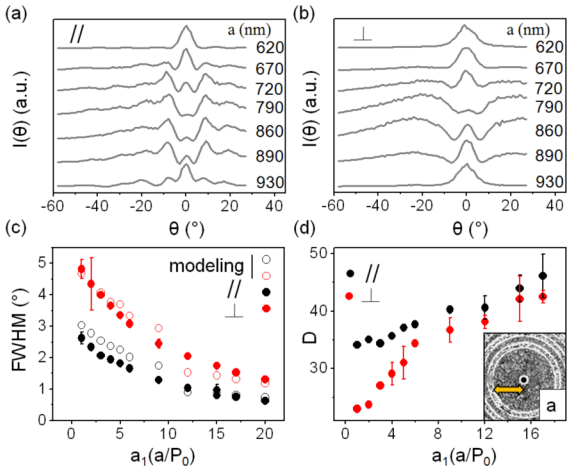

Figure 5. Experimental diffraction patterns recorded at P_0 = 620 nm as a function of a for parallel (a) and perpendicular polarizations (b). fwhm (c) and directivity (d) of resonant BE versus normalized $a_1 = a/P_0$ for both polarizations.

played by the parameter a in the control of the BE antenna. This narrowing directly comes from an increase of the effective coherence length, which is no longer limited by the groove number n, given that the size of the final BE structure for a/P_0 = 20 is approximately 20 μm for P_0 = 620 nm, slightly below l_{SP} = 25 μm. Indeed, within the inner flat cavity defined by a, damping is limited only by ohmic losses and no longer increased by additional scattering losses over the groove corrugations.

In conclusion, we have presented a thorough experimental study of the diffractive properties of BE antennas in the visible, with a special emphasis on the effect of polarization that breaks the cylindrical invariance of the antenna along its optical axis. Carefully analyzed, the impact of the relevant geometrical parameters and the plasmonic near field on the antenna emission can be simply understood from a Huygens−Fresnel approach. We believe that our work opens new perspectives in the control of light with a plasmonic antenna and brings new strategies for the coupling between 2D plasmonic and 3D propagative EM modes. This could notably be applied to spatially deterministic coupling with quantum two-level systems,[33] allowing for a fine control and enhancement of the single photon emission for quantum information transfer.

AUTHOR INFORMATION

Corresponding Author

*E-mail: ebbesen@unistra.fr. Phone: +33 (0)3-68855116. Fax: +33 (0)3-68855161.

Present Address

[⊥]Institut für Physik, Carl von Ossietzky Universität, 26129 Oldenburg, Germany.

Notes

The authors declare no competing financial interest.

ACKNOWLEDGMENTS

We acknowledge support from the ERC (Grant 227557), the French program Investissement d'Avenir (Equipex Union), and the Chinese Scholarship Council (CSC).

REFERENCES

(1) Genet, C.; Ebbesen, T. W. Light in tiny holes. *Nature* **2007**, *445*, 39−46.

(2) Yi, Y.-M.; Cuche, A.; León-Pérez, F.; Degiron, A.; Laux, E.; Devaux, E.; Genet, C.; Alegret, J.; Martín-Moreno, L.; Ebbesen, T. W. Diffraction regimes of single holes. *Phys. Rev. Lett.* **2012**, *109*, 023901.

(3) Laux, E.; Genet, C.; Skauli, T.; Ebbesen, T. W. Plasmonic photon sorters for spectral and polarimetric imaging. *Nat. Photonics* **2008**, *2*, 161−164.

(4) Mahboub, O.; Palacios, S. C.; Genet, C.; García-Vidal, F. J.; Rodrigo, S. J.; Martín-Moreno, L.; Ebbesen, T. W. Optimization of bull's eye structures for transmission enhancement. *Opt. Express* **2010**, *18*, 11292−11299.

(5) Carretero-Palacios, S.; Mahboub, O.; García-Vidal, F. J.; Martín-Moreno, L.; Rodrigo, S. J.; Genet, C.; Ebbesen, T. W. Mechanisms for extraordinary optical transmission through bull's eye structures. *Opt. Express* **2011**, *19*, 10429−10442.

(6) Lezec, H. J.; Degiron, A.; Devaux, E.; Linke, R. A.; Martín-Moreno, L.; García-Vidal, F. J.; Ebbesen, T. W. Beaming light from a subwavelength aperture. *Science* **2002**, *297*, 820−823.

(7) Degiron, A.; Ebbesen, T. W. Analysis of the transmission process through a single aperture surrounded by periodic corrugations. *Opt. Express* **2004**, *12*, 3694−3700.

(8) Martín-Moreno, L.; García-Vidal, F. J.; Lezec, H. J.; Degiron, A.; Ebbesen, T. W. Theory of highly directional emission from a single subwavelength aperture surrounded by surface corrugations. *Phys. Rev. Lett.* **2003**, *90*, 167401.

(9) García-Vidal, F. J.; Martín-Moreno, L.; Lezec, H. J.; Ebbesen, T. W. Focusing light with a single subwavelength aperture flanked by surface corrugations. *Appl. Phys. Lett.* **2003**, *83*, 4500.

(10) Chen, P.; Gan, Q.; Bartoli, F. J.; Zhu, L. Spoof-surface-plasmon assisted light beaming in mid-infrared. *J. Opt. Soc. Am. B* **2010**, *27*, 685−689.

(11) Yu, N.; Wang, Q. J.; Kats, M. A.; Fan, F. A.; Khanna, S. P.; Li, L.; Davies, A. G.; Linfield, E. H.; Capasso, F. Designer spoof surface plasmon structures collimate terahertz laser beams. *Nat. Mater.* **2010**, *9*, 730−735.

(12) Wang, L.; Cao, J. X.; Liu, L.; Lv, Y.; Zheng, S. J. Surface plasmon enhanced transmission and directivity through subwavelength slit in X-band microwaves. *Appl. Phys. Lett.* **2008**, *92*, 241113.

(13) Caglayan, H.; Bulu, I.; Ozbay, E. Plasmonic structures with extraordinary transmission and highly directional beaming properties. *Microwave Opt. Technol. Lett.* **2006**, *48*, 2491−2496.

(14) Greffet, J. J.; Carminati, R.; Joulain, K.; Mulet, J. P.; Mainguy, S.; Chen, Y. Coherent emission of light by thermal sources. *Nature* **2002**, *416*, 61−64.

(15) Fernández-Domínguez, A. I.; Moreno, E.; Martín-Moreno, L.; García-Vidal, F. J. Beaming matter waves from a subwavelength aperture. *Phys. Rev. A* **2006**, *74*, 021601(R).

(16) Christensen, J.; Fernández-Domínguez, A. I.; León-Pérez, F.; Martín-Moreno, L.; García-Vidal, F. J. Collimation of sound assisted by acoustic surface waves. *Nat. Phys.* **2007**, *3*, 851−852.

(17) Guo, B.; Song, G.; Chen, L. Room temperature continuous wave operation of quantum cascade lasers with 12.5% wall plug efficiency. *Appl. Phys. Lett.* **2007**, *91*, 021103.

(18) Yu, N.; Fan, J.; Wang, Q. J.; Pfugl, C.; Diehl, L.; Edamura, T.; Yamanishi, M.; Kan, H.; Capasso, F. Small-divergence semiconductor lasers by plasmonic collimation. *Nat. Photonics* **2008**, *2*, 564−570.

(19) Drezet, A.; Laluet, J. V.; Genet, C.; Ebbesen, T. W. Optical chirality without optical activity: How surface plasmons give a twist to light. *Opt. Express* **2008**, *16*, 12559−12570.

(20) Gorodetski, Y.; Drezet, A.; Genet, C.; Ebbesen, T. W. Generating far-field orbital angular momenta from near-field optical chirality. *Phys. Rev. Lett.* **2013**, *110*, 203906.

(21) Bharadwaj, P.; Deutsch, B.; Novotny, L. Optical antennas. *Adv. Opt. Photon.* **2009**, *1*, 438−483.

(22) Schuller, J. A.; Barnard, E. S.; Cai, W.; Jun, Y. C.; White, J. S.; Brongersma, M. L. Plasmonics for extreme light concentration and manipulation. *Nat. Mater.* **2010**, *9*, 193−204.

(23) Curto, A. G.; Volpe, G.; Taminiau, T. H.; Kreuzer, M. P.; Quidant, R.; Van Hulst, N. F. Unidirectional emission of a quantum dot coupled to a nanoantenna. *Science* **2010**, *329*, 930−933.
(24) Novotny, L.; Van Hulst, N. F. Antennas for light. *Nat. Photonics* **2011**, *5*, 83−90.
(25) Jun, Y. C.; Huang, K. C. Y.; Brongersma, M. L. Plasmonic beaming and active control over fluorescent emission. *Nat. Commun.* **2011**, *2*, 283.
(26) Aouani, H.; Mahboub, O.; Bonod, N.; Devaud, E.; Popov, E.; Rignault, H.; Ebbesen, T. W.; Wenger, J. Bright unidirectional fluorescence emission of molecules in a nanoaperture with plasmonic corrugations. *Nano Lett.* **2011**, *11*, 637−644.
(27) Shin, H.; Catrysse, P. B.; Fan, S. Effect of the plasmonic dispersion relation on the transmission properties of subwavelength cylindrical holes. *Phys. Rev. B* **2005**, *72*, 085436.
(28) Ropers, C.; Park, D. J.; Stibenz, G.; Steinmeyer, G.; Kim, J.; Kim, D. S.; Lienau, C. Femtosecond light transmission and subradiant damping in plasmonic crystals. *Phys. Rev. Lett.* **2005**, *94*, 113901.
(29) Jackson, D. R.; Chen, J. C.; Qiang, R.; Capolino, F.; Oliner, A. A. The role of leaky plasmon waves in the directive beaming of light through a subwavelength aperture. *Opt. Express* **2008**, *16*, 21271−21281.
(30) Hecht, B.; Bielefeldt, H.; Novotny, L.; Inouye, Y.; Pohl, D. W. Local excitation, scattering, and interference of surface plasmons. *Phys. Rev. Lett.* **1996**, *77*, 1889−1892.
(31) Nikitin, A. Y.; Zueco, D.; García-Vidal, F. J.; Martín-Moreno, L. Electromagnetic wave transmission through a small hole in a perfect electric conductor of finite thickness. *Phys. Rev. B* **2008**, *78*, 165429.
(32) Kraus, J. D. *Antennas for All Applications*; McGrawHill: Boston, 2003.
(33) Cuche, A.; Mollet, O.; Drezet, A.; Huant, S. "Deterministic" quantum plasmonics. *Nano Lett.* **2010**, *10*, 4566−4570.